Inorg. Chem. **2003**, *42*, 2764–2773

Redox-Adaptable Copper Hosts. Pyridazine-Linked Cryptands Accommodate Copper in a Range of Redox States

Sally Brooker,*,† Janna D. Ewing,† Tanya K. Ronson,† Charles J. Harding,‡ Jane Nelson,*,§ and David J. Speed‡,§

Department of Chemistry, University of Otago, P.O. Box 56, Dunedin, New Zealand, Chemistry Department, Open University Milton Keynes, MK7 6AA, U.K., and School of Chemistry, Queens University of Belfast, Belfast BT9 5AG, Northern Ireland

Received October 16, 2002

A series of structurally characterized copper complexes of two pyridazine-spaced cryptands in redox states + (I,I), (II,I), (II), (II,II) are reported. The hexaimine cryptand $\mathbf{L_I}$ [formed by the 2 + 3 condensation of 3,6-diformylpyridazine with tris(2-aminoethyl)amine (tren)] is able to accommodate two non-stereochemically demanding copper(I) ions, resulting in $[Cu^{I}_2\mathbf{L_I}](BF_4)_2$ **1**, or one stereochemically demanding copper(II) ion, resulting in $[Cu^{II}\mathbf{L_I}](BF_4)_2$ **3**. Complex **3** crystallizes in two forms, **3a** and **3b**, with differing copper(II) ion coordination geometries. Addition of copper(I) to the monometallic complex **3** results in the mixed-valence complex $[Cu^{I}Cu^{II}\mathbf{L_I}](X)_3$ (X = PF_6^-, **2a**; X = BF_4^-, **2b**) which is well stabilized within this cryptand as indicated by electrochemical studies ($K_{com} = 2.1 \times 10^{11}$). The structurally characterized, octaamine cryptand $\mathbf{L_A}$, prepared by sodium borohydride reduction of $\mathbf{L_I}$, is more flexible than $\mathbf{L_I}$ and can accommodate two stereochemically demanding copper(II) ions, generating the dicopper(II) cryptate $[Cu^{II}_2\mathbf{L_A}](BF_4)_4$ **4**. Electrochemical studies indicate that $\mathbf{L_A}$ stabilizes the copper(II) oxidation state more effectively than $\mathbf{L_I}$; no copper redox state lower than II,II has been isolated in the solid state using this ligand.

Introduction

Rich copper coordination chemistry has resulted from studies employing macrocycles derived from 3,6-diformylpyridazine[1−4] and from cryptands derived from tris(2-aminoethyl)amine (tren).[5−9] In earlier studies[5−13] with hexaiminocryptand ligands we have found that where the spacer links do not incorporate a coordinating donor, copper is accommodated in the +1 redox state (where it is aerobically stable) and utilizes the trigonal pyramidal N4 cap-derived site.[5,6,12] Where N-donors are incorporated into the spacer link, as in the 2,6-pyridino- or 2,5-pyrrole-derived cryptands, the coordination site involves one or more of these N-donors and redox potentials for copper oxidation are less positive; these cryptates are susceptible to aerobic oxidation.[7,10,11] In aminocryptands, where the harder N_{amino} donors are involved in coordination, Cu(II) is the normal redox state, and Cu(I) cryptates are rapidly oxidized in air. Cryptates with inert-spacer links tend to accommodate anions in cascade-binding mode[9] between the pair of Cu(II) ions, whereas this option appears not to be available[10] to pyridino- or pyrrole-spaced analogues because of coordinative saturation and/or the absence of a sterically protected intercationic space. Where steric constraint brings the pair of copper cations into close proximity and in trigonal coordination geometry, a one-

* Authors to whom correspondence should be addressed. E-mail: sbrooker@alkali.otago.ac.nz (S.B.); j.nelson@ulster.ac.uk (J.N.).
† University of Otago.
‡ Open University Milton Keynes.
§ Queens University of Belfast.

(1) Brooker, S.; Kelly, R. J.; Moubaraki, B.; Murray, K. S. *Chem. Commun.* **1996**, 2579−2580.
(2) Brooker, S.; Hay, S. J.; Plieger, P. G. *Angew. Chem., Int. Ed.* **2000**, *39*, 1968−1970.
(3) Brooker, S.; Davidson, T. C.; Hay, S. J.; Kelly, R. J.; Kennepohl, D. K.; Plieger, P. G.; Moubaraki, B.; Murray, K. S.; Bill, E.; Bothe, E. *Coord. Chem. Rev.* **2001**, *216−217*, 3−30.
(4) Brooker, S. *Eur. J. Inorg. Chem.* **2002**, 2535−2547.
(5) Harding, C.; McKee, V.; Nelson, J. *J. Am. Chem. Soc.* **1991**, *113*, 9684−9685.
(6) Lu, Q.; Latour, J. M.; Harding, C. J.; Martin, N.; Marrs, D. J.; McKee, V.; Nelson, J. *J. Chem. Soc., Dalton Trans.* **1994**, 1471−1478.
(7) Lu, Q.; McKee, V.; Nelson, J. *J. Chem. Soc., Chem. Commun.* **1994**, 649−651.
(8) Al-Obaidi, A.; Baranovic, G.; Coyle, J.; Coates, C. G.; McGarvey, J. J.; McKee, V.; Nelson, J. *Inorg. Chem.* **1998**, *37*, 3567−3574.
(9) Nelson, J.; McKee, V.; Morgan, G. *Prog. Inorg. Chem.* **1998**, *47*, 167−317.
(10) Marrs, D. J.; McKee, V.; Nelson, J.; Lu, Q.; Harding, C. J. *Inorg. Chim. Acta* **1993**, *211*, 195−202.
(11) Qin, L.; McCann, M.; Nelson, J. *J. Inorg. Biochem.* **1993**, *51*, 633−639.
(12) Harding, C. J.; Lu, Q.; Malone, J. F.; Marrs, D. J.; Martin, N.; McKee, V.; Nelson, J. *J. Chem. Soc., Dalton Trans.* **1995**, 1739−1747.
(13) Arnaud-Neu, F.; Fuangswasdi, S.; Maubert, B.; Nelson, J.; McKee, V. *Inorg. Chem.* **2000**, *39*, 573−579.

10.1021/ic0261124 CCC: $25.00
Published on Web 03/21/2003

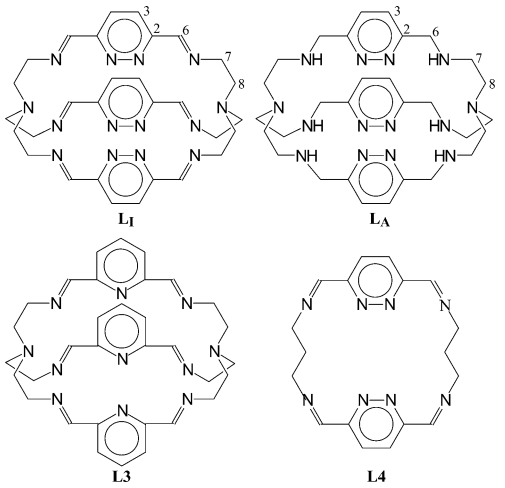

Figure 1. The cryptands, $\mathbf{L_I}$ and $\mathbf{L_A}$, used in this work, along with the **L3** and **L4** ligands reported previously in the literature.

electron copper−copper bond is formed which generates the average-valence dicopper(1.5) redox state. This average-valence state is present and moderately stable in both hexaimino and octaamino cryptand hosts which have a 2-carbon spacer.[5,8] However in the smallest hexaimino (2-carbon spaced) host, it is also possible to isolate a mono-copper(II) cryptate, depending on synthetic conditions used such as stoichiometry and choice of solvent.

Apart from our earlier work,[14,15] there is only one previous mention of a cryptand containing the potentially important pyridazine spacer,[16] so we wished to explore the copper chemistry of the cryptand derived from 3,6-diformylpyridazine and tris(2-aminoethyl)amine (tren), $\mathbf{L_I}$ (Figure 1). The synthesis and characterization of $\mathbf{L_I}$ and of the $[Co^{II}\mathbf{L_I}](BF_4)_2$ **5**, $[Co^{II}Cu^{I}\mathbf{L_I}](BF_4)_3$ **6**, and $[Cu^{II}Cu^{I}\mathbf{L_I}](PF_6)_3$ **2a** complexes was reported recently.[14,15] Here we present the copper coordination chemistry of the hexaimine cryptand $\mathbf{L_I}$ and of the related octaamine cryptand $\mathbf{L_A}$ (Figure 1). Cryptand $\mathbf{L_A}$, generated by sodium borohydride reduction of $\mathbf{L_I}$, was prepared in order to provide a more flexible and more chemically stable host (hexaimine crypts such as $\mathbf{L_I}$ can be prone to hydrolytic breakdown[12,13]). In addition, it was anticipated that the redox properties of the resulting copper complexes would respond to replacement of $\mathbf{L_I}$ by $\mathbf{L_A}$ thus widening the available redox range. The synthesis and structural, electrochemical, magnetic, and ESR characterization of $[Cu^{I}_2\mathbf{L_I}](BF_4)_2$ **1**, $[Cu^{I}Cu^{II}\mathbf{L_I}](X)_3$ (X = PF_6^-, **2a**; X = BF_4^-, **2b**), $[Cu^{II}\mathbf{L_I}](BF_4)_2$ **3**, and $[Cu^{II}_2\mathbf{L_A}](BF_4)_4$ **4** are reported (Scheme 1).

Results and Discussion

Synthesis. The hexaimine cryptand, $\mathbf{L_I}$, was prepared as previously described.[14] The sodium borohydride reduction of $\mathbf{L_I}$ produced the octaamine analogue, $\mathbf{L_A}$, in good yield (Scheme 1).

Scheme 1

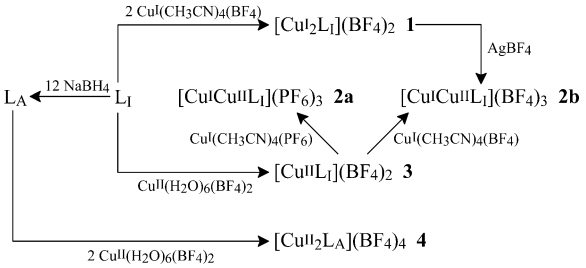

As it had been observed that two non-stereochemically demanding ions, silver(I) ions, could be accommodated by $\mathbf{L_I}$,[14] an attempt was made to encapsulate two copper(I) ions. The reaction of 2 equiv of $[Cu^{I}(CH_3CN)_4]BF_4$ with $\mathbf{L_I}$ in methanol under argon gave $[Cu^{I}_2\mathbf{L_I}](BF_4)_2$ **1** as a brown powder, in 70−80% yield. This is consistent with previous results which have showed that tren-derived hexaimine cryptands are effective hosts for Cu(I).[10,11]

When this experiment was carried out in air, a brown powder was obtained which, in a low-yielding recrystallization from acetonitrile by diethyl ether diffusion, gave $[Cu^{I}Cu^{II}\mathbf{L_I}](PF_6)_3$ **2a** as a brown crystalline solid. This mixed-valence complex was subsequently prepared in improved yield by reacting $\mathbf{L_I}$ with 1 equiv of copper(II) ions followed by 1 equiv of copper(I) ions. In this case, for convenience, the BF_4^- derivative $[Cu^{I}Cu^{II}\mathbf{L_I}](BF_4)_3$ **2b** was isolated. In addition we were able to show, via ESR monitoring, that the mixed-valence cryptates can also be obtained by Ag^+ oxidation of the dicopper(I) analogues.

The reaction of 1 equiv of copper(II) tetrafluoroborate with $\mathbf{L_I}$ in acetonitrile and a small amount of ethanol gave on slow evaporation $[Cu^{II}\mathbf{L_I}](BF_4)_2$ **3** as a green crystalline solid in 56% yield. In some preparations small amounts of brown hexagon and lime green plate crystals were obtained in addition to the green rod crystals. The elemental analysis of this mixture was the same as that of **3**, and indeed all three crystal forms have this stoichiometry. Single-crystal X-ray structure determinations have shown that the brown hexagons and green rods **3a** are isomorphous, whereas in the lime green plates **3b** the copper(II) ion is in a different coordination environment (see later).

Attempts to include a second copper(II) ion did not lead to isolation of a clean product. Nor did use of 2:1 stoichiometry combined with rapid isolation of the product lead to isolation of a characterizable dicopper(II) cryptate. FAB-MS showed sizable additional peaks corresponding to $\mathbf{L_I}\cdot H_2O$ fragments which suggest ring opening, and IR spectra showed an amine band at 3245 cm^{-1} and a high ν shoulder on the imine band which may correspond to C=O stretching. The difficulty in obtaining a pure sample of the dicopper-(II) cryptate is consistent with our expectation[14,15] that $\mathbf{L_I}$ cannot bind a second stereochemically demanding metal ion. However, isolation of **3** in pure form indicates that the pyridazine-spaced cryptand $\mathbf{L_I}$ is better suited to the accommodation of copper(II) than the analogous pyridine-spaced hexaimine cryptand, **L3** (Figure 1), which is unable to generate even monocopper(II) cryptates in pure form.[10]

(14) Brooker, S.; Ewing, J. D.; Nelson, J. *Inorg. Chim. Acta* **2001**, *317*, 53−58.
(15) Brooker, S.; Ewing, J. D.; Nelson, J.; Jeffery, J. C. *Inorg. Chim. Acta* **2002**, *337*, 463−466.
(16) Lehn, J.-M. *Supramolecular Chemistry*; VCH: New York, 1995.

The reaction of the octaamine cryptand, $\mathbf{L_A}$, with 2 equiv of copper(II) tetrafluoroborate salt gave $[Cu^{II}_2\mathbf{L_A}](BF_4)_4$ **4** as blue crystals, in 85% yield. One drop of triethylamine was added prior to the addition of the copper(II) salt to prevent the formation of a partially protonated green byproduct. The yield of this synthesis was found to be highly dependent on the amount of TEA added. Attempts at forming a monocopper(II) complex of $\mathbf{L_A}$ were unsuccessful; both the blue powdery first crop and green powdery second crop analyzed as complex mixtures.

Infrared spectra of **1**−**4** confirmed that the $\mathbf{L_I}$ cryptand remained intact in **1**−**3** (imine at 1638 cm^{-1} for **1**, 1637 cm^{-1} for **2a,** and 1647 cm^{-1} for **3**), that the $\mathbf{L_A}$ cryptand is present in **4** (N−H stretch, 3283 cm^{-1}; N−H bending, weak band at 1632 cm^{-1}), and confirmed the presence of the expected anions (1083 cm^{-1} for **1**, 843 and 559 cm^{-1} for **2a**, 1083 for **2b**, 1052 cm^{-1} for **3**, and 1059 cm^{-1} for **4**). In each case the microanalyses and FAB mass spectra were consistent with the proposed formulas. FAB mass spectra (see Experimental Section) confirmed the formulation of **1**−**4** via the observation of a monopositive cryptate ion, usually formed via loss of one cation. The dicopper cryptates **1** and **2b** both show a cluster at 718 for $[Cu_2\mathbf{L_I}]$ and a weaker $[Cu^{II}_2\mathbf{L_A}](BF_4)$ cluster. The FAB mass spectrum of **3** had a strong signal corresponding to the monocopper cryptate (no anions) and a peak for $\mathbf{L_I}$. Strong signals for the successive loss of the tetrafluoroborate anions from $Cu_2\mathbf{L_A}(BF_4)_3$ were followed by a weak signal for the loss of one of the copper ions in the FAB mass spectrum of **4**.

The molar conductivity values of 300 mol^{-1} cm^2 Ω^{-1} for **1** and 263 mol^{-1} cm^2 Ω^{-1} for **3** in acetonitrile are consistent with the literature range for a 2:1 electrolyte (220−300 mol^{-1} cm^2 Ω^{-1}), while the value of 391 mol^{-1} cm^2 Ω^{-1} obtained for **2a** in acetonitrile is typical for a 3:1 (340−420 mol^{-1} cm^2 Ω^{-1}) electrolyte.[17] The molar conductivity of **4**, 462 mol^{-1} cm^2 Ω^{-1}, is significantly higher than that of the literature range for a 3:1 (340−420 mol^{-1} cm^2 Ω^{-1}) electrolyte, suggesting that the product behaves as a 4:1 electrolyte in solution as expected.

The UV/visible spectrum of $\mathbf{L_I}$ in dichloromethane has an intense $\pi-\pi^*$ transition at 248 nm (ϵ = 61500 L mol^{-1} cm^{-1}). The dicopper(I) complex (**1**) in acetonitrile has in addition to a similar $\pi-\pi^*$ absorption at 245 nm (ϵ = 47500 L mol^{-1} cm^{-1}) a less intense metal-to-ligand charge-transfer band at 390 nm (ϵ = 3960 L mol^{-1} cm^{-1}). The UV/visible spectrum of **2b** in acetonitrile has a band at 734 nm (ϵ = 98 L mol^{-1} cm^{-1}) which corresponds to the d−d transition of the Cu(II) ion. As for the dicopper(I) complex (**1**), an intense $\pi-\pi^*$ band is observed for **2b** at 245 nm (ϵ = 45000 L mol^{-1} cm^{-1}). The UV/visible spectrum of **3** in MeCN has an asymmetric band at 776 nm (ϵ = 95 L mol^{-1} cm^{-1}), a longer wavelength than was observed for the mixed-valence complex **2b**, which is attributed to the d−d transition of the distorted octahedral copper(II) ion. As seen for **1** and **2b**, an intense $\pi-\pi^*$ transition is observed for **3** at 246 nm (ϵ = 45100 L mol^{-1} cm^{-1}). The UV/visible spectrum of the dicopper(II) complex of the octaamine cryptand (**4**) has a band at 631 nm (ϵ = 550 L mol^{-1} cm^{-1}) which is assigned to the d−d transitions of the copper(II) centers and indicates that the $\mathbf{L_A}$ ligand exerts a stronger field than $\mathbf{L_I}$. There is also an intense $\pi-\pi^*$ band at 272 nm (ϵ = 90100 L mol^{-1} cm^{-1}), red-shifted from the hexaimino analogue.

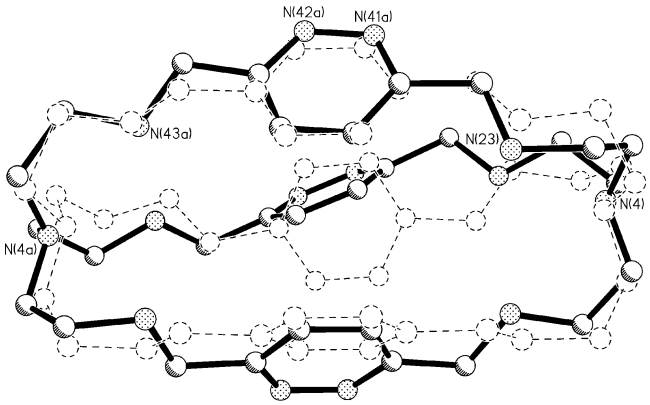

Figure 2. Perspective view of the amine cryptand, $\mathbf{L_A}$ (solid lines), overlaid on that of $\mathbf{L_I}$ (dotted lines). The labeled atoms are those used in the least-squares fit of the two structures to one another.

Crystal Structures. Crystals of $\mathbf{L_A}$ were obtained from chloroform by vapor diffusion of diethyl ether, and the structure was determined. For comparison purposes the structure is displayed overlaid on that of $\mathbf{L_I}$ (Figure 2). Due to conjugation the pyridazine diimine units in $\mathbf{L_I}$ are fairly flat, whereas in $\mathbf{L_A}$ the amine single bonds are twisted well out of the respective pyridazine ring planes. This is particularly clear when one compares the conformation of the central strands in Figure 2: in contrast to the almost planar pyridazine diamine unit in $\mathbf{L_I}$, in $\mathbf{L_A}$ the C−N bonds in the central strand are at almost 45° to the plane of the pyridazine ring [torsion angles: N(1)−C(5)−C(6)−N(3) −130.8(2)°, N(41a)−C(42a)−C(26)−N(23) −167.0(1)°, N(42)−C(45)−C(46)−N(43) 160.1(1)°]. The $N_{bridgehead}\cdots N_{bridgehead}$ distance [10.767(5) Å] in $\mathbf{L_A}$ is somewhat longer than that observed in $\mathbf{L_I}$ [10.443(7) Å]. Another difference between the two structures is that there are a number of intra- and intermolecular hydrogen bonds present in the structure of $\mathbf{L_A}$ whereas none are observed for $\mathbf{L_I}$. It is noticeable that the pyridazine octaamine cryptand, in contrast to other octaamine cryptands which have been structurally characterized,[5−9] is not well preorganized for complexation on account of the transoid disposition of amine and pyridazine donors. This is most pronounced in the top and bottom strands [the N(41) and N(41a) rings are related by symmetry]. In the central strand the almost 45° twist of the imine bond out of the plane of the pyridazine ring reduces the appropriateness of this comparison.

Brown crystals of $[Cu^{I}_2\mathbf{L_I}](BF_4)_2$ **1** were grown by diethyl ether diffusion into a chloroform/acetonitrile/ethanol solution of **1**, and the crystal structure was determined (Figure 3 and Table 1). The copper(I) ions are located within the tetraamine-derived caps, achieving their preferred distorted trigonal pyramidal geometry by coordination of the three imine nitrogen donors and the bridgehead nitrogen atom although the interactions with the imine nitrogen donors are

(17) Geary, W. J. *Coord. Chem. Rev.* **1971**, *7*, 81−122.

Table 1. Selected Bond Lengths (Å) and Angles (deg) for Compounds **1**, **2a**, **3a**, **3b**, and **4**

	1	**2a**	**3a**	**3b**	**4**
Cu(1)−N(1)		1.990(3)			
Cu(1)−N(21)		2.017(3)			
Cu(1)−N(23)	1.998(4)	1.979(5)			2.287(3)
Cu(1)−N(3)	2.045(4)	2.003(5)			2.002(3)
Cu(1)−N(43)	2.045(3)	2.006(5)			2.622(3)
Cu(1)−N(4)	2.247(3)	2.292(5)			2.052(3)
Cu(2)−N(22)		2.047(5)		2.493(3)	
Cu(2)−N(2)		2.347(6)		2.138(3)	
Cu(2)−N(46)	1.994(3)	2.238(6)	1.966(3)	2.074(3)	2.049(3)
Cu(2)−N(6)	2.018(4)	2.048(5)	1.994(3)	2.221(3)	2.193(3)
Cu(2)−N(42)		2.102(5)	2.076(3)	2.086(3)	2.014(3)
Cu(2)−N(26)	2.033(3)	2.107(5)	2.214(3)	2.048(3)	2.101(3)
Cu(2)−N(5)	2.248(3)	2.051(3)	2.155(3)		
N(4)...N(5)	10.969(5)	10.306(8)	10.478(9)	10.587(5)	9.016(9)
Cu(1)...Cu(2)	6.478(1)	4.960(2)			5.874(2)
N(1)−Cu(1)−N(3)					82.46(13)
N(1)−Cu(1)−N(21)					94.75(12)
N(1)−Cu(1)−N(4)					163.19(14)
N(1)−Cu(1)−N(23)					110.25(12)
N(1)−Cu(1)−N(43)					90.95(12)
N(3)−Cu(1)−N(21)					176.64(13)
N(21)−Cu(1)−N(4)					96.83(13)
N(21)−Cu(1)−N(23)					76.79(12)
N(21)−Cu(1)−N(43)					87.66(11)
N(23)−Cu(1)−N(3)	129.64(14)	120.9(2)			102.38(13)
N(23)−Cu(1)−N(43)	113.96(14)	121.1(2)			154.42(12)
N(23)−Cu(1)−N(4)	85.01(13)	83.6(2)			84.33(13)
N(3)−Cu(1)−N(4)	82.36(13)	80.8(2)			86.30(14)
N(3)−Cu(1)−N(43)	112.26(14)	112.5(2)			94.23(12)
N(43)−Cu(1)−N(4)	82.27(13)	81.9(2)			77.41(12)
N(22)−Cu(2)−N(6)		162.1(2)		161.79(11)	
N(22)−Cu(2)−N(42)		89.0(2)		78.75(11)	
N(22)−Cu(2)−N(26)		78.3(2)		74.30(12)	
N(22)−Cu(2)−N(46)		95.9(2)		91.29(11)	
N(22)−Cu(2)−N(2)		87.3(2)		86.46(12)	
N(6)−Cu(2)−N(2)		74.8(2)		75.35(13)	
N(42)−Cu(2)−N(2)		90.4(2)		84.98(12)	
N(26)−Cu(2)−N(2)		96.0(2)		91.84(12)	
N(46)−Cu(2)−N(2)		164.47(19)		163.75(12)	
N(46)−Cu(2)−N(6)	121.48(14)	101.3(2)	140.09(13)	105.91(12)	101.63(13)
N(46)−Cu(2)−N(42)		74.5(2)	79.26(12)	78.80(13)	82.28(13)
N(6)−Cu(2)−N(42)		90.9(2)	100.81(12)	98.42(12)	108.60(12)
N(46)−Cu(2)−N(26)	111.19(14)	99.5(2)	106.78(12)	103.05(12)	138.55(13)
N(6)−Cu(2)−N(26)	123.30(14)	103.4(2)	105.68(11)	106.70(12)	116.38(12)
N(42)−Cu(2)−N(26)		165.4(2)	124.25(11)	153.00(12)	99.64(12)
N(5)−Cu(2)−N(26)	82.67(13)		79.55(13)		83.77(13)
N(46)−Cu(2)−N(5)	83.79(13)		80.93(12)		84.16(13)
N(6)−Cu(2)−N(5)	83.50(14)		82.76(11)		84.31(13)
N(42)−Cu(2)−N(5)			152.70(12)		162.89(13)

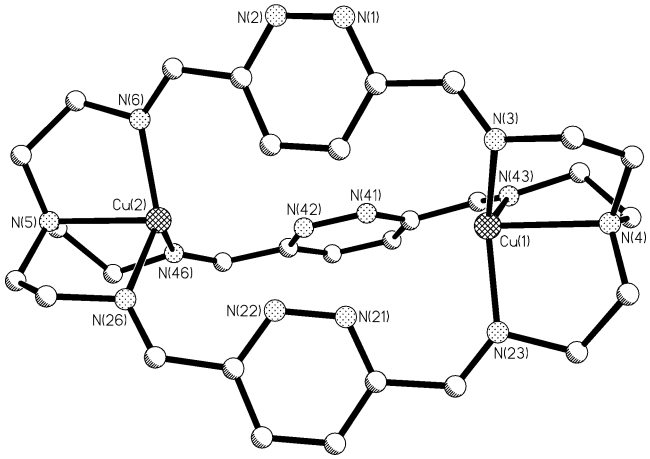

Figure 3. Perspective view of the cation, $[Cu^{I}_{2}\mathbf{L_I}]^{2+}$, of **1**.

stronger than those to the bridgehead atoms (average Cu−N_{imine} = 2.02 Å, average Cu−$N_{bridgehead}$ = 2.25 Å). As observed for the copper(I) ion in the structure of **2a**,[15] Cu(1) and Cu(2) in **1** are out of the $(N_{imine})_3$ mean planes, by 0.238 and 0.234 Å, respectively, away from the bridgehead nitrogen atoms, N(4) and N(5), respectively. In the dicopper(I) cryptate of the pyridine-spaced analogue of $\mathbf{L_I}$, **L3** (Figure 1), the Cu(I) ions are more severely displaced from the $(N_{imine})_3$ mean plane (Cu···$N_{bridgehead}$ = 2.75 Å) because of hemicoordination of the pyridine N-donors.[10] In contrast, there are no bonding interactions with the linker heteroatoms in **1** [shortest Cu−$N_{pyridazine}$ = 3.073 Å, for Cu(2)−N(42)]. The $N_{bridgehead}$···$N_{bridgehead}$ distance [10.969(5) Å] is increased over that of the free $\mathbf{L_I}$ cryptand [10.443(7) Å] and is also larger than that in the mixed-valence complex **2a** [10.306-(8) Å]. The interatomic spacing of the copper ions in the dicopper(I) complex **1** is also significantly greater than in the mixed-valence complex **2a** [Cu(1)···Cu(2) = 6.478(1) Å for **1** and 4.960(2) Å for **2a**].

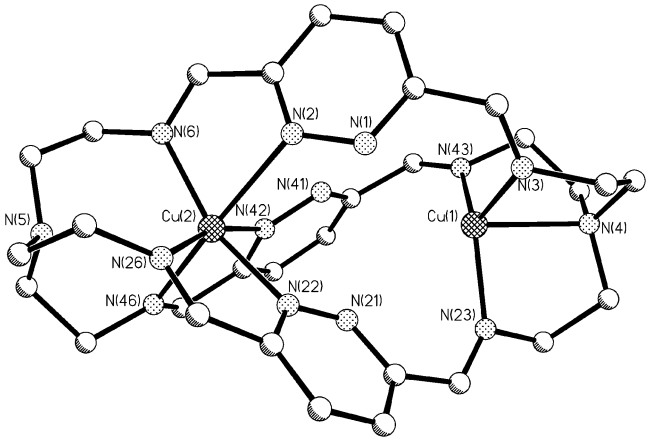

Figure 4. Perspective view of the mixed-valence cation, $[Cu^{II}Cu^{I}\mathbf{L_I}]^{3+}$, of **2a**.

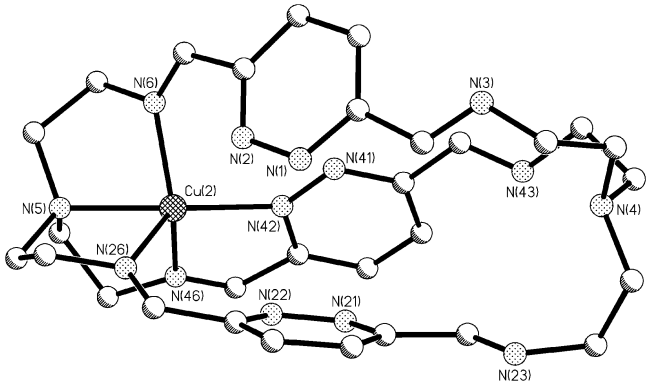

Figure 5. Perspective view of the cation, $[Cu^{II}\mathbf{L_I}]^{2+}$, of **3a** (green rods).

Brown crystals of $[Cu^{I}Cu^{II}\mathbf{L_I}](PF_6)_3$ **2a** were grown by the slow diffusion of diethyl ether vapor into an acetonitrile solution, and the crystal structure was determined (Figure 4 and Table 1) and has been reported.[15] Here one nitrogen atom from each of the three pyridazine moieties is coordinated to the Cu(II) cation in this localized mixed-valence cryptate. As is the case with complex **1**, the conformation of the cryptand host, $\mathbf{L_I}$, in **2a** is such that the imine CN functions within a strand are mutually cis to the pyridazine CN bonds. Comparison of the structures of **2a** and **5** indicates that it should be possible to encapsulate a second non-stereochemically demanding ion, such as copper(I), in **5** to make a heterodimetallic cryptand complex. This has subsequently been proven with the formation of $[Co^{II}Cu^{I}\mathbf{L_I}](BF_4)_3$.[15]

Crystals of $[Cu^{II}\mathbf{L_I}](BF_4)_2$ **3** were grown by the slow diffusion of diethyl ether vapor into an acetonitrile solution. The crystal structure was determined for all three of the observed crystal forms. The brown hexagons were shown to be isomorphous with the green rods **3a**, whereas a different copper(II) ion geometry is observed in the lime green plates **3b** (Figures 5 and 6 and Table 1). In the green rods, **3a**, the copper(II) ion has a distorted trigonal bipyramidal environment as a consequence of binding to all three of the imine nitrogen atoms, the nitrogen bridgehead atom, and just one pyridazine nitrogen atom (Figure 5). The next-nearest $Cu(2)\cdots N_{pyridazine}$ [to N(2)] is 3.097 Å. It is interesting to note that the copper(II) ion in the mononuclear complex **3a** is five-coordinate whereas in the binuclear complex **2a** it is six coordinate. The coordination of the copper ion has not changed the $N_{bridgehead}\cdots N_{bridgehead}$ distance of the cryptand by much [10.478(9) Å in **3a** vs 10.443(7) Å in $\mathbf{L_I}$].[14]

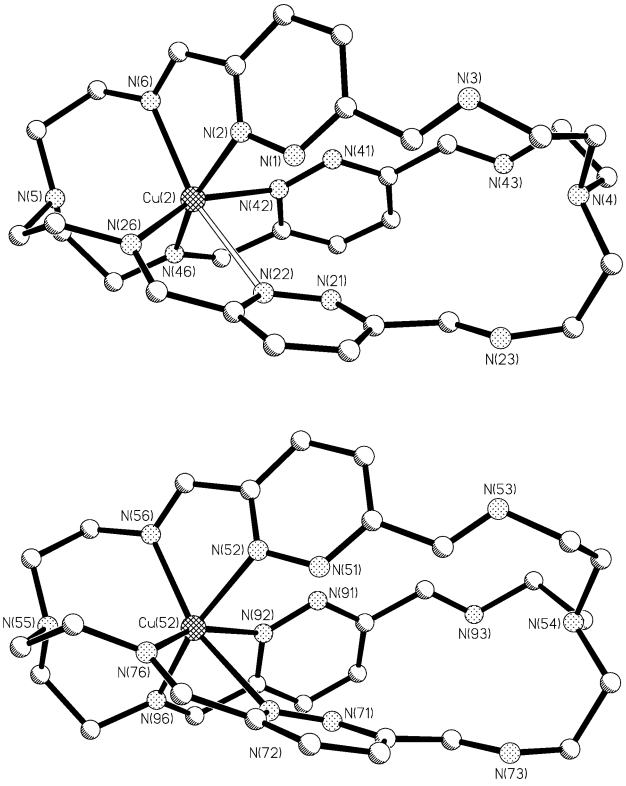

Figure 6. Perspective views of the two independent cations, $[Cu^{II}\mathbf{L_I}]^{2+}$, of **3b** (lime green plates). Selected bond lengths (Å) and angles (deg) for the second cryptate (bottom) in the asymmetric unit: Cu(52)−N(76) 2.041(3), Cu(52)−N(92) 2.085(3), Cu(52)−N(96) 2.088(3), Cu(52)−N(52) 2.170(3), Cu(52)−N(56) 2.205(3), Cu(52)−N(72) 2.395(3), N(76)−Cu(52)−N(92) 155.42(13), N(76)−Cu(52)−N(96) 101.55(13), N(92)−Cu(52)−N(96) 78.47(13), N(76)−Cu(52)−N(52) 92.37(12), N(92)−Cu(52)−N(52) 85.71(12), N(96)−Cu(52)−N(52) 164.15(12), N(76)−Cu(52)−N(56) 106.36(13), N(92)−Cu(52)−N(56) 96.80(12), N(96)−Cu(52)−N(56) 107.85(13), N(52)−Cu(52)−N(56) 74.86(13), N(76)−Cu(52)−N(72) 75.44(13), N(92)−Cu(52)−N(72) 79.98(12), N(96)−Cu(52)−N(72) 89.31(12), N(52)−Cu(52)−N(72) 86.87(13), N(56)−Cu(52)−N(72) 161.66(12).

In contrast, in the lime green plates **3b**, the copper(II) ion is in a distorted octahedral environment, having bound three imine nitrogen atoms and, in this case, three pyridazine nitrogen atoms (Figure 6). There are two independent cryptates in the asymmetric unit, and there are some slight differences between them (Table 1 and Figure 6 caption). The coordination of the copper ion in this different binding mode has caused a slight lengthening of the $N_{bridgehead}\cdots N_{bridgehead}$ distance of the cryptand [10.478(9) Å in **3a** vs 10.587(5) and 10.501(5) Å in **3b**].

As with $[Co^{II}\mathbf{L_I}](BF_4)_2$ **5**,[14] $\mathbf{L_I}$ has demonstrated some flexibility in being able to accommodate a single stereochemically demanding ion. However, the structures of **3a, 3b**, and **5** have both similarities and differences. The cobalt(II) ion has a six-coordinate environment [φ (twist angle) = 46.9°; φ = 60° for octahedral, 0° for trigonal prismatic[9]] intermediate between octahedral and trigonal prismatic which is rather similar to that adopted by the copper(II) ion in both **3b** [φ = 45.8, 46.7°] and **2a** [φ = 45.4°], rather than a five-coordinate environment, as adopted by copper(II) in **3a**.

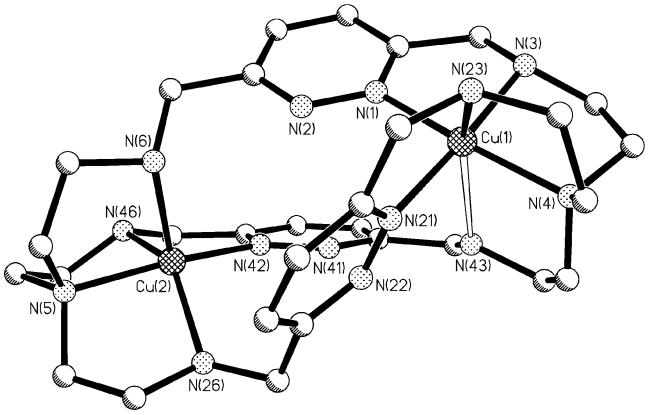

Figure 7. Perspective view of the cation, $[Cu^{II}_2\mathbf{L_A}]^{4+}$, of **4**.

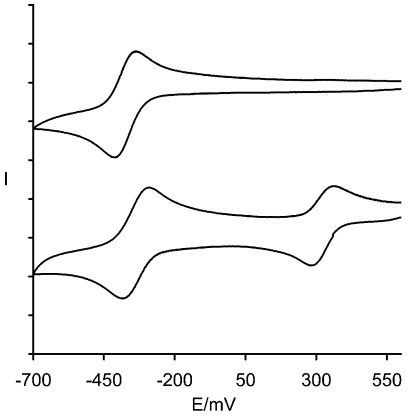

Figure 8. Cyclic voltammograms of complexes **1** (bottom) and **3** (top) in acetonitrile (200 mV s^{-1}, vs 0.01 mol L^{-1} $AgNO_3$/Ag).

Comparing the two mononuclear copper(II) structures, in both cases the copper ions coordinate to three imine nitrogen donors, but in **3b** it also binds three pyridazine rings whereas in **3a** it binds just one pyridazine nitrogen donor and a $N_{bridgehead}$ donor atom. Within the mononuclear structures **3a**, **3b**, and **5** each of the three strands of the organic host has all trans conformations of the imine bonds. These strands would therefore have to change their conformations to all cis before a second metal cation could coordinate.

Blue crystals of $[Cu^{II}_2\mathbf{L_A}](BF_4)_4$ **4** were grown by the vapor diffusion of diethyl ether into an acetonitrile solution, and the crystal structure was determined (Figure 7 and Table 1). As we have seen in the hexaimine cryptate series, pyridazine N donors, despite their relative "softness", are acceptable to and utilized by Cu(II). The copper(II) ions have slightly different environments from one another: Cu(1) binds to one nitrogen bridgehead atom, two pyridazine nitrogen atoms, and two amine nitrogen atoms whereas Cu(2) binds to one nitrogen bridgehead atom, one pyridazine nitrogen atom, and three amine nitrogen atoms. Cu(1) interacts weakly with the amine nitrogen atom N(43) [2.622(3) Å], and correspondingly it is not displaced much from the N(1)N(3)N(4)N(21) plane of donors toward N(23) [0.094(2) Å]. In comparison, the square pyramidal copper (II) ion, Cu(2), is significantly displaced from the N(5)N(26)N(41)N(46) plane of donors toward N(6) [0.406(2) Å]. Interestingly, the metal ions are not bridged by any of the three pyridazine rings as each ring coordinates via only one nitrogen atom, not both. The coordination of two Cu(II) cations requires tranformation of the amine and pyridazine N donors from the *transoid* disposition of the free ligand to *cisoid* in two of the three strands, while the third, very nonplanar strand is best described as *cis, trans*.

The increased flexibility of the $\mathbf{L_A}$ host, over that of $\mathbf{L_I}$, is clearly illustrated by the fact that it has managed to encapsulate these two stereochemically demanding transition metal ions. The absence of π-conjugation in each aminopyridazine strand allows twisting, which is particularly noticeable in one part of the third strand [N(22)−C(22)−C(31)−N(26) 108.4(4)°; cf.: the range of the remaining five $N_{pyridazine}-C_{pyridazine}-C_{imine}-N_{imine}$ torsion angles is 9.3(5)−25.6(5)°], to ensure this outcome. The copper−copper separation in **2a** is shorter than that in **4** [Cu(1)···Cu(2) is 4.960-(2) Å in **2a** vs 5.874(2) Å in **4**] while the $N_{bridgehead}\cdots N_{bridgehead}$ distance is longer [N(4)···N(5) is 10.306(8) Å in **2a** vs 9.016-(9) Å in **4**].

Electrochemical Studies on 1−4. On the basis of our experience with dicopper complexes of the related pyridazine-containing tetraimine macrocycle **L4** (Figure 1), which include dicopper(II), dicopper(I), and mixed-valence copper(II)copper(I) complexes,[1−3] we expected lower oxidation states to be stabilized by this pyridazine-containing cryptand $\mathbf{L_I}$, as is observed. All potentials are quoted vs 0.01 M $AgNO_3$/Ag unless otherwise stated.

The cyclic voltammogram of $[Cu^{I}_2\mathbf{L_I}](BF_4)_2$ **1** (Figure 8) reveals two reversible one-electron waves, at $E_{1/2} = -0.34$ V ($\Delta E = 0.08$ V) and $E_{1/2} = +0.33$ V ($\Delta E = 0.09$ V). Controlled potential electrolysis experiments first at 0.00 V and then at 0.50 V resulted in the addition of 0.99 electron equiv and then a further 0.96 electron equiv, confirming that both processes are one-electron processes. The redox process at $E_{1/2} = -0.34$ V is therefore assigned as $Cu^ICu^I \leftrightarrow Cu^I$-$Cu^{II}$, and the process at $E_{1/2} = +0.33$ V is assigned as Cu^I-$Cu^{II} \leftrightarrow Cu^{II}Cu^{II}$. The cyclic voltammogram was unchanged 10 min after these Coulombic experiments, indicating that the green oxidation product, $[Cu^{II}_2\mathbf{L_I}]^{4+}$, was at least the major constituent under the strictly anhydrous conditions used. On scanning to below −0.8 V, however, we observed a stripping wave at −0.48 V on the return scan.

Although **1** is stable in the solid state in air these electrochemical studies indicate that molecular oxygen should be capable of oxidizing **1** to the mixed-valence cryptate **2**. Consistent with this we have been able to prepare **2a** from copper(I) starting materials by carrying out the reaction and subsequent recrystallization in air. This pyridazine-spaced cryptand, $\mathbf{L_I}$, thus appears to be a less effective host for copper(I) ions than the relatively O_2-insensitive pyridine-spaced analogue **L3**.[10]

As anticipated, the cyclic voltammogram of the mixed-valence cryptate, $[Cu^ICu^{II}\mathbf{L_I}](BF_4)_3$ **2b**, is very similar in appearance to that of **1** (Figure 8): two reversible one-electron waves are observed at $E_{1/2} = -0.34$ V ($\Delta E = 0.08$ V) and $E_{1/2} = +0.33$ V ($\Delta E = 0.08$ V). Controlled potential electrolysis experiments were performed, the first at −0.55 V followed by a second on this reduced solution at +0.40

V. The former resulted in the addition of 0.80 electron equiv, and the latter resulted in the removal of 1.93 electron equiv and the dark yellow-brown solution becoming pale green in color. Again the $[Cu^{II}_2\mathbf{L_I}]^{4+}$ product appeared to be intact at the conclusion of these coulometric experiments as there was no change in the cyclic voltammogram. These processes are assigned as for **1** (see above). Despite both of the observed waves being due to one-electron processes, the $Cu^ICu^{II} \leftrightarrow Cu^{II}Cu^{II}$ process always had significantly lower peak currents than those observed for the $Cu^ICu^I \leftrightarrow Cu^ICu^{II}$ process: this may be due to increased electrostatic repulsion between the electrode and the more highly charged cryptate in that case.

In the cyclic voltammogram of $[Cu^{II}\mathbf{L_I}](BF_4)_2$ **3** in MeCN, upon scanning to negative potentials (Figure 8), one reversible reduction wave is observed, at $E_{1/2} = -0.38$ V ($\Delta E =$ 0.08 V), which is assigned to the $Cu^{II} \leftrightarrow Cu^I$ redox process. A controlled potential coulometric experiment, performed at −0.70 V, took 10 min and resulted in the addition of 0.95 electron equiv, confirming that this is a one electron reduction process. The stability of the resulting dark yellow-brown reduction product, under argon, was illustrated by the fact that the cyclic voltammogram was initially unchanged, although the reduction product was unstable over time with some precipitation of copper metal occurring. Scanning to potentials below −1.4 V causes further reduction of the Cu(I) ions and consequently the observation of a stripping wave at −0.61 V. On scanning to positive potentials a series of irreversible processes occurs above +0.80 V.

Comparison of the K_{com} values estimated[18] from the cyclic voltammetry results for **1** and **2** with those obtained for the $[Cu^{II}_2\mathbf{L4}(MeCN)_2](ClO_4)_4$ complex[1−3] in which the mixed-valence Cu^ICu^{II} state is stabilized in acetonitrile, between −0.15 and +0.20 V ($K_{com} = 8.3 \times 10^5$), and isolable, reveals that the $\mathbf{L_I}$ cryptand is better able to stabilize such a mixed-valence species ($K_{com} = 2.1 \times 10^{11}$). The ability of these two cyclic pyridazine-containing ligands, **L4** and $\mathbf{L_I}$, to stabilize mixed-valence dicopper complexes contrasts with the results generally obtained for acyclic pyridazine-containing ligands.[4,19−22] The **L4** macrocycle stabilizes the mixed-valence dicopper species to a similar extent as the (2 + 2) Schiff base macrocycle derived from 2,6-diformyl-4-methylphenol and 1,3-diaminopropane does,[23−25] so the $\mathbf{L_I}$ cryptand is also superior, in this regard, to this macrocyclic phenolate ligand system. The $\mathbf{L_I}$ cryptand is also better able to stabilize the mixed-valence species than is the analogous pyridine-spaced cryptand, **L3**. For the latter cryptand the mixed-valence state is stabilized between −0.110 and +0.012 V vs Fc^+/Fc ($K_{com} = 7.7 \times 10^3$) and has not been isolated from solution.[10] The wide stability range of the one-electron dicopper reductant/oxidant, **2**, makes it attractive as a mild redox agent for nonaqueous use.

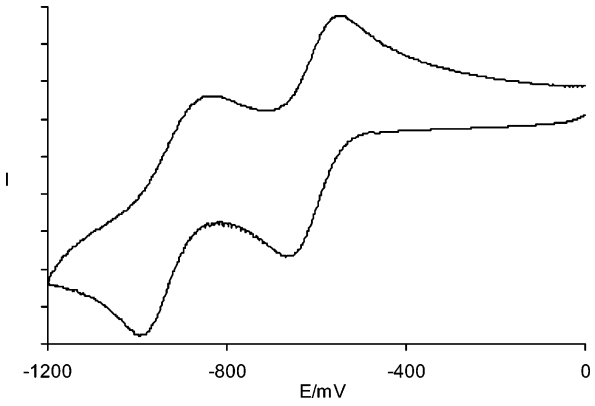

Figure 9. Cyclic voltammograms of complex **4** in acetonitrile (200 mV s^{-1}, vs 0.01 mol L^{-1} $AgNO_3$/Ag).

Above +1.0 V, the cyclic voltammograms of **1**, **2b**, **3,** and $[Co^{II}\mathbf{L_I}]^{2+}$ **5** are quite similar, all showing the same, presumably ligand-based, processes.

The cyclic voltammogram of **4** shows no significant processes on scanning to positive potentials, except for an irreversible oxidation wave at about +1.20 V which is most likely to be due to ligand oxidation. The simplicity of this region is in stark contrast to complexity observed with complexes of the $\mathbf{L_I}$ ligand, which suggests hexaimine cryptand instability when coordinated to metal(II) ions.

On scanning to negative potentials, two one-electron quasi-reversible processes are observed for **4** (Figure 9). The first wave occurs at $E_{1/2} = -0.61$ V ($\Delta E = 0.12$ V) and is associated with the addition of 0.97 electron equiv (controlled potential electrolysis at −0.78 V). The second wave occurs at $E_{1/2} = -0.93$ V ($\Delta E = 0.15$ V) and is of similar height to the first wave. These reduction processes are probably metal centered: $Cu^{II}Cu^{II} \leftrightarrow Cu^ICu^{II}$ at −0.61 V and $Cu^ICu^{II} \leftrightarrow Cu^ICu^I$ at −0.93 V ($K_{com} = 2.6 \times 10^5$). On scanning to more negative potentials, beyond −1.40 V, a stripping wave occurs at −0.55 V on the return cycle indicating that further reduction results in the deposition of copper on the electrode. As expected,[12] these results show that the octaamine ligand $\mathbf{L_A}$ is more effective in stabilizing copper(II) than the hexaimine ligand $\mathbf{L_I}$. In particular, we note that the reduced degree of stabilization of the mixed-valence form, when combined with the significantly lower redox potential, is probably sufficient to make its isolation in the solid state problematic.

Magnetism and ESR Spectroscopy. Magnetic studies and ESR spectroscopy serve to confirm the oxidation states of copper in these compounds, and ESR establishes the classification of the mixed-valence complex.

Complex **1** is effectively diamagnetic with a magnetic susceptibility of a few percent of that expected from a Cu(II) ion, indicating a small paramagnetic impurity. This is confirmed by the ESR spectrum, which indicates traces of a Cu(II) complex at about 1%. In accord with the formulation

(18) Richardson, D. E.; Taube, H. *Inorg. Chem.* **1981**, *20*, 1278−1285.
(19) Zhang, Y.; Thompson, L. K.; Bubenik, M.; Bridson, J. N. *J. Chem. Soc., Chem. Commun.* **1993**, 1375−1377.
(20) Chen, L.; Thompson, L. K.; Bridson, J. N. *Inorg. Chim. Acta* **1993**, *214*, 67−76.
(21) Chen, L.; Thompson, L. K.; Bridson, J. N. *Inorg. Chem.* **1993**, *32*, 2938−2943.
(22) Chen, L.; Thompson, L. K.; Bridson, J. N. *Inorg. Chim. Acta* **1996**, *244*, 87−93.
(23) Gagne, R. R.; Koval, C. A.; Smith, T. J.; Cimolino, M. C. *J. Am. Chem. Soc.* **1979**, *101*, 4571−4580.
(24) Gagne, R. R.; Henling, L. M.; Kistenmacher, T. J. *Inorg. Chem.* **1980**, *19*, 1226−1231.
(25) Mandal, S. K.; Thompson, L. K.; Newlands, M. J.; Gabe, E. J. *Inorg. Chem.* **1989**, *28*, 3707−3713.

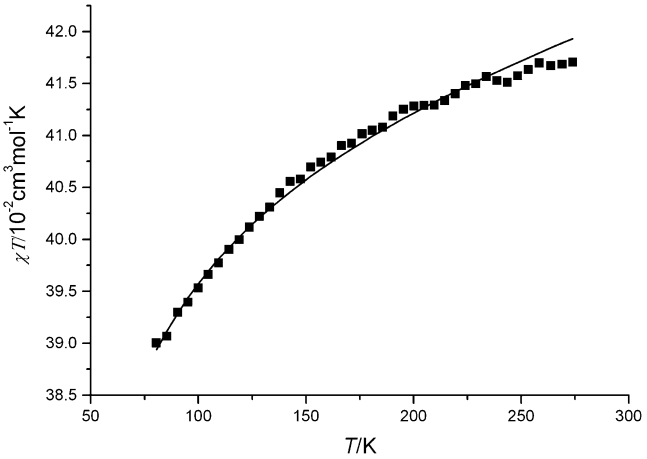

Figure 10. Plot of χT versus T for **4**; the line is the theoretical fit.

of **2a**, the magnetic moment at room temperature is 2.06 μ_B per complex. At 120 K the ESR spectrum of a DMF glass has a 4-line parallel with $g = 2.28$, $A = 138$ G and a broad perpendicular line at $g = 2.09$. In the Robin and Day classification,[26] this behavior is characteristic of class I, in which the four-line hyperfine shows the unpaired electron to remain fully localized, here to temperatures at least as high as 120 K. Of the many mixed-valence dicopper complexes known, this is the most common type.[27]

Complex **3** has a temperature-independent magnetic moment of 1.90 μ_B per complex, and the ESR spectrum is typical of mononuclear copper: a 4-line parallel ($g = 2.27$, $A = 135$ G) and broad perpendicular line ($g = 2.10$).

Complex **4** has weakly interacting dicopper(II) centers (Figure 10). The room temperature magnetic moment is slightly suppressed (1.83 μ_B per copper ion) and falls steadily as T is reduced, to a value of 1.77 μ_B per copper ion at 80 K. In this range, the magnetic data fit the Hamiltonian ($H = -2JS_1 \cdot S_2$) with parameters of $2J = -13.2 \pm 0.2$ cm^{-1}, $g = 2.09$ with T. I. P. at 60×10^{-6} cm^3 mol^{-1}. At 150 K, the ESR spectrum of a DMF glass has a very weak half band at g of 4.23 with typical low hyperfine splitting (78 G). The parallel feature at g of 2.22 shows similar splitting running into a broad perpendicular line at $g = 2.09$. The weak antiferromagnetic exchange observed for **4** is as might be expected, given the lack of bridging moieties between the copper(II) ions (Figure 6). This situation is similar to that applying in the dicopper(II) pyridine-spaced octaamine cryptate analog of **L3** ($-2J \approx 20$ cm^{-1}) but contrasts with the strong antiferromagnetic coupling, $-2J = 482$ cm^{-1}, observed in the $[Cu^{II}_2\mathbf{L4}(MeCN)_2](ClO_4)_4$ complex due to the effective overlap of the copper $d_{x^2-y^2}$ orbitals with the bridging pyridazine orbitals in this near-coplanar conformation.[1−3]

Conclusion

As anticipated, the use of the potentially binucleating $\mathbf{L_I}$ cryptand as a host has proved to be very interesting as a variety of occupancies have been observed. Further evidence that only a single stereochemically demanding metal ion can be bound is found in the isolation of **3** in a state of high purity from 1:1 Cu(II):$\mathbf{L_I}$ stoichiometry in contrast to the impure partly ring-opened or reduced products which result from 2:1 stoichiometry. The binding of such a metal ion alters the conformation of the cryptand so that a second stereochemically demanding metal ion cannot bind. This opens up two important possibilities: the formation of mixed-metal complexes,[15] which will be the topic of a separate paper,[28] and the formation of mixed-valence complexes.[15] The latter possibility has been demonstrated by the formation of **2** where a copper(II) center binds to one site (distorted octahedral), preventing the binding of a second copper(II) center but allowing a non-stereochemically demanding copper(I) center to occupy the second binding site (distorted trigonal pyramidal). ESR studies performed on **2a** at low temperatures revealed that it is a class I mixed-valence complex with the unpaired electron localized on one of the copper centers, as expected from the structure determination, and reported previously.[15] The redox behavior of these two complexes, and other complexes, of $\mathbf{L_I}$ showed very similar oxidative processes above +1.0 V, which are believed to be ligand-centered. The reversible wave observed for the monocopper(II) complex **3** (−0.38 V) and one of the two reversible waves observed for the dicopper complexes **1** and **2b** (−0.34 V) occur at similar potentials and are assigned to $Cu^I \leftrightarrow Cu^{II}$ redox processes, $Cu^I \leftrightarrow Cu^{II}$ and $Cu^ICu^I \leftrightarrow Cu^ICu^{II}$, respectively. In contrast, the second reversible wave observed for **1** and **2b** occurs at a much more positive potential, +0.33 V. It is also assigned to a $Cu^I \leftrightarrow Cu^{II}$ process, specifically, $Cu^ICu^{II} \leftrightarrow Cu^{II}_2$. Clearly the two copper centers in **1** and **2** do interact and the mixed-valence state is significantly stabilized ($K_{com} = 2.1 \times 10^{11}$). The existence of a chemically stable one-electron transfer redox agent capable of reduction and oxidation under mild conditions may have useful applications.

The octaamine $\mathbf{L_A}$ host was found to be significantly more flexible. Unlike the hexaimine $\mathbf{L_I}$ host, $\mathbf{L_A}$ can readily encapsulate two stereochemically demanding copper(II) ions. While the details of the coordination environments differ somewhat, both copper(II) ions have distorted square pyramidal coordination geometries. The copper centers do not coordinate to the same pyridazine rings, so pyridazine bridging is not observed and hence only very weak antiferromagnetic coupling of the Cu(II) paramagnets is observed. The results of the cyclic voltammetry studies show, as anticipated, that the octaamine cryptand, $\mathbf{L_A}$, stabilizes the copper(II) ions much more effectively than the hexaimine cryptand, $\mathbf{L_I}$. The mixed-valence state is much less well stabilized within $\mathbf{L_A}$ ($K_{com} = 2.6 \times 10^5$).

Experimental Section

Materials. 3,6-Diformylpyridazine,[29] $\mathbf{L_I}$,[14] and $Cu^I(MeCN)_4X$ (X = PF_6 or BF_4)[30] were made as previously described. For the electrochemical studies HPLC grade MeCN was distilled from CaH_2

(26) Robin, M. B.; Day, P. *Adv. Inorg. Chem. Radiochem.* **1967**, *10*, 247−422.
(27) Dunaj-Jurco, M.; Ondrejovic, G.; Melnik, M.; Garaj, J. *Coord. Chem. Rev.* **1988**, *83*, 1−28.
(28) Brooker, S.; Ronson, T. K.; Nelson, J. Unpublished work.
(29) Brooker, S.; Kelly, R. J. *J. Chem. Soc., Dalton Trans.* **1996**, 2117−2122.
(30) Kubas, G. J. *Inorg. Synth.* **1990**, *28*, 68.

immediately before use. Chloroform was extracted with the equivalent volume of water, four times, and dried over Na_2SO_4, before use. All other solvents and reagents were used as received.

Measurements were made as previously described[29] except for the following: the electrochemistry and spectroelectrochemistry was carried out, with 1 mmol L^{-1} dry acetonitrile solutions and 0.1 mol L^{-1} tetraethylammonium perchlorate or tetrabutylammonium hexafluorophosphate supporting electrolyte, on an EG&G Princeton Applied Research 273A potentiostat using a 0.01 mol L^{-1} $AgNO_3$/Ag reference electrode. As a further reference check, ferrocene was added at the conclusion of each experiment: the Fc/Fc^+ couple consistently occurred at $E_{1/2} = +0.07 \pm 0.01$ V with $\Delta E = 0.07$ V. The ESR spectra were obtained on an X-band Varian E109 spectrometer. Magnetic measurements were carried out using an Oxford Instruments Faraday magnetic susceptibility balance with a resistive electromagnet operating at 0.8 T (8000 G), and an Oxford Systems cryostat employed as a temperature control down to 80 K. All magnetic data were corrected for diamagnetic contributions using Pascal's constants.

L_A. L_I (0.593 g, 1 mmol) was suspended in 400 mL of methanol and stirred for 15 min before sodium borohydride (0.454 g, 12 mmol) was added in small portions over a period of 2 h. The mixture clarified on addition of the reductant, and was stirred for 2 days before the methanol was removed in vacuo. The resulting white powder was dissolved in 80 mL of water and extracted with chloroform using a continuous extractor (three extractions each of 1 h duration). The extracts were combined, and the chloroform was removed in vacuo to yield **L_A** as a white powder (0.465 g, 77%). Recrystallization from chloroform by vapor diffusion of diethyl ether gives starlike clusters of colorless single crystals. (Found: C, 59.36; H, 7.71; N, 32.37. Calcd for $C_{30}H_{48}N_{14}$: C, 59.58; H, 8.00; N, 32.42.) ν_{max}/cm^{-1} (KBr disk, inter alia): 3441 (w), 3243 (m), 2809 (m), 1467 (sh), 1448 (s), 1434 (sh), 1325 (s), 1124 (ss), 829 (s). ^1H NMR (300 MHz, solvent $CHCl_3$, reference TMS): δ 7.26 (1H, s, H_3), 3.98 (2H, s, H_6), 2.87 (2H, t, H_8), 2.71 (2H, t, H_7), 2.08 (1H, s br, NH). ^{13}C NMR (75 MHz, solvent $CDCl_3$, reference $CDCl_3$): δ 160.3 (C_2), 125.9 (C_3), 53.5 (C_6), 53.0 (C_7), 47.8 (C_8). FAB *m*/*z* (fragment): 605 [$C_{30}H_{49}N_{14}$], 303 [$C_{30}H_{50}N_{14}$]. λ_{max}/nm (MeCN) (ϵ/dm^3 mol^{-1} cm^{-1}): ~253sh (6130), 309 (1270).

$[Cu^I_2L_I](BF_4)_2$ 1. L_I (0.058 g, 0.1 mmol) was suspended in methanol (30 mL). Solid $Cu^I(CH_3CN)_4BF_4$ (0.062 g, 0.2 mmol) was added to the suspension under argon, causing the mixture to clarify and become dark brown. After stirring for 2 h the mixture was filtered to yield the product as a brown powder (0.076 g, 87%). Crystals suitable for X-ray analysis were obtained by diethyl ether diffusion into a chloroform/acetonitrile/ethanol solution of **1**. (Found: C, 40.30; H, 3.93; N, 21.57. Calcd for $Cu_2C_{30}H_{36}N_{14}(BF_4)_2$: C, 40.33; H, 4.06; N, 21.95.) ν_{max}/cm^{-1} (KBr disk, inter alia): 3424 (b), 1638 (mw), 1083 (s), 1034 (s), 521 (w). Swansea FAB *m*/*z* (fragment): 805w [$Cu_2C_{30}H_{36}N_{14}(BF_4)$], 718 [$Cu_2C_{30}H_{36}N_{14}$], 655 [$CuC_{30}H_{36}N_{14}$]. ^1H NMR (500 MHz, solvent CD_3CN, reference CH_3CN): at 298 K, δ 8.43 (1H, s br, H_6), 7.98 (1H, s, H_3), 3.85 (2H, t, H_7), 3.09 (2H, t, H_8); at 243 K, δ 8.492 (1H, s br), 8.016 (1H, s br), 3.949 (s br), 3.184 (s br). ^{13}C NMR (126 MHz, solvent CD_3CN, reference CD_3CN): δ 160.8 (C_6), 156.5 (C_2), 128.4 (C_3), 59.0 (C_7), 53.2 (C_8). $\mu = 0.00\ \mu_B$ (298 K). λ_{max}/nm (MeCN) (ϵ/dm^3 mol^{-1} cm^{-1}): 245 (47500), 390 (3960). Λ_m(MeCN) = 300 mol^{-1} cm^2 Ω^{-1} (1:2 = 220−300 mol^{-1} cm^2 Ω^{-1}, 1:3 = 340−420 mol^{-1} cm^2 Ω^{-1}).[17]

$[Cu^ICu^{II}L_I](PF_6)_3$ 2a: as described above for **1** but carried out in air and using $Cu^I(CH_3CN)_4PF_6$. The brown powder obtained from the reaction solution was recrystallized in air from MeCN by vapor diffusion of diethyl ether to give a small amount of brown crystals of **2a**. (Found: C, 32.73; H, 3.40; N, 17.10. Calcd for $Cu_2C_{30}H_{36}N_{14}(PF_6)_3$: C, 32.14; H, 3.29; N, 17.57.) ν_{max}/cm^{-1} (KBr disk, inter alia): 3412 (b, s), 1641 (w), 841 (b, s) 556 (s). $\mu = 2.06\ \mu_B$ per complex (298 K).

$[Cu^ICu^{II}L_I](BF_4)_3$ 2b. Method (a). L_I (0.058 g, 0.1 mmol) was suspended in dry acetonitrile (50 mL) and stirred. To this was added an acetonitrile solution (10 mL) of $Cu^{II}(BF_4)_2 \cdot 4H_2O$ (0.030 g, 0.1 mmol), causing the suspension to clarify and become green. After stirring for 30 min the mixture was filtered to remove a small amount of unreacted **L_I**. Solid $Cu^I(CH_3CN)_4BF_4$ (0.030 g, 0.1 mmol) was then added to the mixture, causing it to become dark brown. After stirring overnight the volume was reduced to about 20 mL. Diethyl ether diffusion into the resulting solution gave brown crystals of **2b** (0.081 g, 83%). (Found: C, 36.76; H, 3.81; N, 19.82. Calcd for $Cu_2C_{30}H_{36}N_{14}(BF_4)_3$: C, 36.76; H, 3.70; N, 20.01). ν_{max}/cm^{-1} (KBr disk, inter alia): 3418 (b, s), 1637 (w), 1083 (s), 531 (w). FAB *m*/*z* (fragment): 805 [$Cu_2C_{30}H_{36}N_{14}(BF_4)$], 718 [$Cu_2C_{30}H_{36}N_{14}$], 655 [$CuC_{30}H_{36}N_{14}$]. λ_{max}/nm (MeCN) (ϵ/dm^3 mol^{-1} cm^{-1}): 246 (45000), 734 (98). Λ_m(MeCN) = 391 mol^{-1} cm^2 Ω^{-1} (1:3 = 340−420 mol^{-1} cm^2 Ω^{-1}).[17]

Method (b). To 20 mg of **1** in 20 mL of MeCN was added 4.3 mg of $AgBF_4$ as a solid, and an immediate lightening of the dark brown color was noted. The solvent volume was reduced under N_2, the solution filtered to remove Ag(s), and the filtrate allowed to concentrate to very low volume under N_2. Around 3−4 mg of brown product was isolated which showed an ESR spectrum identical with that of a characterized sample of **2b**.

$[Cu^{II}L_I](BF_4)_2$ 3. L_I (0.060 g, 0.1 mmol) was added to an acetonitrile solution (15 mL) of $Cu^{II}(BF_4)_2 \cdot 4H_2O$. The resulting pale green suspension clarified upon rapid stirring. After stirring for 30 min the mixture was filtered to remove a small amount of unreacted **L_I** and ethanol (4 mL) added to the filtrate. Slow evaporation of the acetonitrile/ethanol solution gave **3** as a green crystalline solid. The solid was removed by filtration, washed with 3 mL of ethanol, and dried in vacuo (0.059 g, 68%). Green single crystals were obtained by vapor diffusion of diethyl ether into a green acetonitrile solution of **3** (0.047 g, overall yield 56%). In some preparations brown hexagon crystals and lime green plate crystals were obtained in addition to the green rod crystals. However, the presence of the brown crystals did not significantly affect the elemental analysis and a small % of copper(I) doping into the crystal form is suspected. (Found: C, 43.60; H, 4.39; N, 23.51. Calcd for $Cu_1C_{30}H_{36}N_{14}(BF_4)_2$: C, 43.42; H, 4.37; N, 23.63). ν_{max}/cm^{-1} (KBr disk, inter alia): 3442 (b), 2849 (s), 1647 (s), 1052 (s). Swansea FAB *m*/*z* (fragment): 655 [$CuC_{30}H_{48}N_{14}$], 594 [$C_{30}H_{48}N_{14}$]. λ_{max}/nm (MeCN) (ϵ/dm^3 mol^{-1} cm^{-1}): 246 (45100), 776 (95). $\mu = 1.90\ \mu_B$ (280 K). Λ_m(MeCN) = 263 mol^{-1} cm^2 Ω^{-1} (1:2 = 220−300 mol^{-1} cm^2 Ω^{-1}, 1:3 = 340−420 mol^{-1} cm^2 Ω^{-1}).[17]

$[Cu^{II}_2L_A](BF_4)_4$ 4. L_A (0.046 g, 0.08 mmol) was dissolved into 25 mL of methanol and was stirred. To this was added one drop of triethylamine followed by a methanol solution (5 mL) of $Cu^{II}(BF_4)_2 \cdot 4H_2O$ (0.047 g, 0.16 mmol). Upon addition of the copper salt, the clear solution changed to a deep blue color. After stirring for 2 h, the solution was filtered, yielding a blue powder (0.07 g, 85%). Blue single crystals can be obtained by recrystallization from acetonitrile by vapor diffusion of diethyl ether. (Found: C, 33.39; H, 4.48; N, 18.17. Calcd for $Cu_2C_{30}H_{48}N_{14}(BF_4)_4$: C, 33.43; H, 4.53; N, 18.21). ν_{max}/cm^{-1} (KBr disk, inter alia): 3396 (b), 3283 (m), 1635 (w), 1465 (s), 1445 (s), 1059 (s, b), 521 (w, s). Swansea FAB *m*/*z* (fragment): 991 [$Cu_2C_{30}H_{48}N_{14}(BF_4)_3$], 904 [$Cu_2C_{30}H_{48}N_{14}(BF_4)_2$], 818 [$Cu_2C_{30}H_{48}N_{14}BF_4$], 729 [$Cu_2C_{30}H_{48}N_{14}$], 665 [$CuC_{30}H_{48}N_{14}$]. λ_{max}/nm (MeCN) (ϵ/dm^3 mol^{-1} cm^{-1}): 272 (90100), 631

(550). $\mu = 1.83\ \mu_B$ per Cu (280 K), $-2J = 13.2\ cm^{-1}$. Λ_m(MeCN) = 462 $mol^{-1}\ cm^2\ \Omega^{-1}$ (1:3 = 340−420 $mol^{-1}\ cm^2\ \Omega^{-1}$).[17]

X-ray Crystallography. Data were collected on Bruker SMART diffractometers, using graphite-monochromated Mo Kα radiation (λ = 0.71013 Å). The data were corrected for Lorentz and polarization effects, and semiempirical absorption corrections were applied. The structures were solved by direct methods (SHELXS-97)[31,32] and refined against all F^2 data (SHELXL-97).[33] Hydrogen atoms were inserted at calculated positions (except where noted) and rode on the atoms to which they are attached (including isotropic thermal parameters which were equal to 1.2 times the equivalent isotropic displacement parameter for the attached non-hydrogen atom), and all non-hydrogen atoms were made anisotropic.

Crystal Data for L_A: $C_{30}H_{48}N_{14}$, colorless plate, 0.40 × 0.24 × 0.10 mm^3, monoclinic, space group $C2/c$, a = 28.801(14) Å, b = 8.656(4) Å, c = 14.854(6) Å, β = 119.083(10)°, V = 3236(3) $Å^3$, μ = 0.080 mm^{-1}, Z = 4, $F(000)$ = 1304, T = 163 K; 20071 reflections were collected, and the 3269 independent reflections were used in the analysis. The nitrogen hydrogen atoms were located from difference maps and then rode on the nitrogen atoms to which they are attached. The refinement of 200 parameters converged to R1 = 0.0394 [for 1998 reflections having $I > 2\sigma(I)$], wR2 = 0.1000, and goodness of fit 0.911 (for all 3269 data).

Crystal Data for $[Cu_2L_I](BF_4)_2$ 1: $C_{30}H_{36}B_2Cu_2F_8N_{14}$, yellow-brown plate, 0.43 × 0.36 × 0.03 mm^3, triclinic, space group $P\bar{1}$, a = 8.6996(9) Å, b = 14.4770(14) Å, c = 14.7656(15) Å, α = 77.724(2)°, β = 74.268(2)°, γ = 85.530(2)°, V = 1748.6(3) $Å^3$, μ = 1.307 mm^{-1}, Z = 2, $F(000)$ = 908, T = 153 K; 17036 reflections were collected, and the 6148 independent reflections were used in the analysis. The disordered tetrafluoroborate ion was restrained to be like the full-occupancy one using the SAME instruction. The refinement of 541 parameters converged to R1 = 0.0554 [for 4477 reflections having $I > 2\sigma(I)$], wR2 = 0.1430, and goodness of fit 0.983 (for all 6148 F^2 data).

Crystal Data for $[CuL_I](BF_4)_2$ 3a: $C_{30}H_{36}B_2CuF_8N_{14}$, green rod, 0.51 × 0.19 × 0.14 mm^3, monoclinic, space group $P2(1)/n$, a = 14.259(14) Å, b = 11.940(11) Å, c = 21.20(2) Å, β = 100.997(11)°, V = 3543(6) $Å^3$, μ = 0.705 mm^{-1}, Z = 4, $F(000)$ = 1700, T = 163 K; 27290 reflections were collected, and the 7204 independent reflections were used in the analysis. The refinement of 496 parameters converged to R1 = 0.0444 [for 7204 reflections having $I > 2\sigma(I)$], wR2 = 0.0800, and goodness of fit 0.779 (for all 7204 F^2 data).

(31) Sheldrick, G. M. *Acta Crystallogr., Sect. A* **1990**, *46*, 467−473.
(32) Sheldrick, G. M. *Methods Enzymol.* **1997**, *276*, 628−641.
(33) Sheldrick, G. M.; Schneider, T. R. *Methods Enzymol.* **1997**, *277*, 319−343.

Crystal Data for $[CuL_I](BF_4)_2$ 3b: $C_{30}H_{36}B_2CuF_8N_{14}$, lime green plate, 0.43 × 0.35 × 0.08 mm^3, triclinic, space group $P\bar{1}$, a = 9.400(4) Å, b = 13.640(5) Å, c = 29.938(12) Å, α = 82.694(5)°, β = 86.851(6)°, γ = 75.134(5)°, V = 3679(2) $Å^3$, μ = 0.679 mm^{-1}, Z = 4, $F(000)$ = 1700, T = 168 K; 47333 reflections were collected, and the 14607 independent reflections were used in the analysis. The refinement of 991 parameters converged to R1 = 0.0505 [for 6354 reflections having $I > 2\sigma(I)$], wR2 = 0.1476, and goodness of fit 0.817 (for all 14607 F^2 data).

Crystal Data for $[Cu_2L_A](BF_4)_4 \cdot 0.5CH_3CN \cdot H_2O$ 4·0.5CH_3CN·H_2O: $C_{33}H_{54.5}B_4Cu_2F_{16}N_{15.5}O$, blue plate, 0.50 × 0.22 × 0.07 mm^3, monoclinic, space group $C2/c$, a = 22.769(11) Å, b = 11.974(4) Å, c = 36.121(14) Å, β = 97.881(9)°, V = 9755(7) $Å^3$, μ = 0.981 mm^{-1}, Z = 8, F(000) = 4728, T = 163 K; 63878 reflections were collected, and the 11020 independent reflections were used in the analysis. The nitrogen and O80 hydrogen atoms were located from difference maps, and then rode on the nitrogen atoms to which they are attached, with the exception of H43N and H80A, which were fixed. Hydrogen atoms could not be found for the half-occupancy water molecule, O90, and so were not included. The half-occupancy acetonitrile molecule was restrained to be like the full-occupancy one using the SAME instruction. The refinement of 665 parameters converged to R1 = 0.0535 [for 11020 reflections having $I > 2\sigma(I)$], wR2 = 0.1464, and goodness of fit 0.968 (for all 11020 F^2 data).

CCDC reference numbers: 195441−195445.

Acknowledgment. S.B. thanks the University of Otago for the granting of study leave which facilitated the initial drafting of this manuscript, and gratefully acknowledges her host J.N. and the financial support of a Queens University Belfast Visiting Professorship. We are grateful to Dr. J. Wikaira and Professor W. T. Robinson (University of Canterbury) for the X-ray data collections on **L_A**, **3a**, **3b**, and **4**, and to Dr. M. Nieuwenhuyzen (Queens University Belfast) for providing access to the diffractometer for the data collection on **1**. We acknowledge the EPSRC Swansea FAB mass spectrometry service (Swansea) and B. M. Clark (University of Canterbury) for the mass spectra and thank Associate Professor A. J. McQuillan (University of Otago) for helpful discussions.

Supporting Information Available: Crystallographic data for **L_A**, **1**, **3a**, **3b**, and **4·0.5CH_3CN·H_2O**, in CIF format. This material is available free of charge via the Internet at http://pubs.acs.org.

IC0261124